



HAL
open science

Experimental design approach for the synthesis of 3D-CoFe₂O₄ nanoflowers thin films by low-cost process

Nabil Hosni, Karim Zehani, Kais Djebali, Frédéric Mazaleyrat, Lotfi Bessais,
Hager Maghraoui-Meherzi

► To cite this version:

Nabil Hosni, Karim Zehani, Kais Djebali, Frédéric Mazaleyrat, Lotfi Bessais, et al.. Experimental design approach for the synthesis of 3D-CoFe₂O₄ nanoflowers thin films by low-cost process. *Materials Chemistry and Physics*, 2020, 255, pp.123493. 10.1016/j.matchemphys.2020.123493 . hal-03389420

HAL Id: hal-03389420

<https://hal.science/hal-03389420>

Submitted on 26 Apr 2024

HAL is a multi-disciplinary open access archive for the deposit and dissemination of scientific research documents, whether they are published or not. The documents may come from teaching and research institutions in France or abroad, or from public or private research centers.

L'archive ouverte pluridisciplinaire **HAL**, est destinée au dépôt et à la diffusion de documents scientifiques de niveau recherche, publiés ou non, émanant des établissements d'enseignement et de recherche français ou étrangers, des laboratoires publics ou privés.

Experimental Design Approach for the Synthesis of 3D-CoFe₂O₄ nanoflowers thin films by low-cost process

N. Hosni^a, K. Zehani^b, K. Djebali^c, F. Mazaleyrat^d, L. Bessais^b, Hager Maghraoui-Meherzi^a

^a University of Tunis El Manar, Faculty of Science, Laboratory of Analytical Chemistry and Electrochemistry, Campus, LR99ES15, 2092 Tunis, Tunisia.

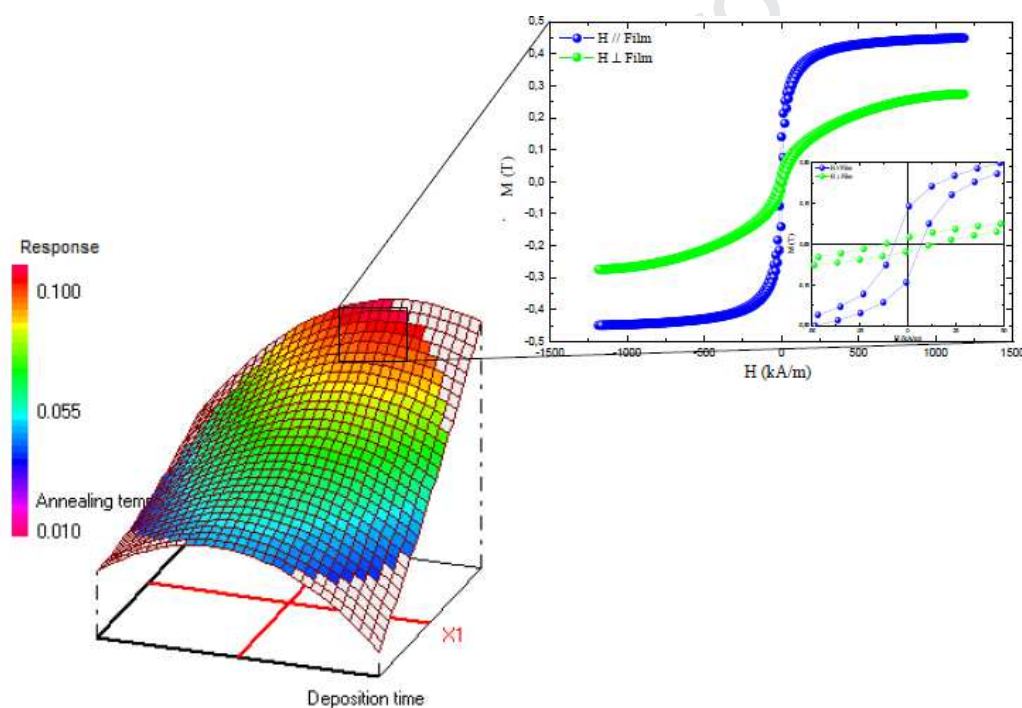
* Corresponding author: e-mail: nabil.hosni@fst.utm.tn

^b Univ Paris Est Creteil, CNRS, ICMPE, 2 rue Henri Dunant, 94320 Thiais, France

^c Laboratory of Useful Materials Valuation, National Center for Research in Materials Sciences, Borj Cedria Technopark, Soliman, Tunisia

^d SATIE, ENS Paris-Saclay, CNRS, Universite Paris-Saclay, 4 avenue des sciences, 91190 Gif-sur-Yvette, France.

Graphical abstract



Highlights

- 3D-CoFe₂O₄ nanoflowers thin films was successfully synthesized by low-cost chemical bath deposition (CBD) process
- Rechtschaffner design has been applied to investigate the influence of the principal experimental parameters on saturation magnetization.
- Doehlert matrix has been used to predict the optimal condition of the saturation magnetization.
- The obtained 3D-CoFe₂O₄ nanoflowers thin film could be useful for supercapacitor application.

Abstract

Three-dimensional CoFe_2O_4 nanoflowers thin films have been deposited on stainless steel by low-cost chemical bath deposition process. The experimental design methodology has been applied to investigate the effect of the principal experimental parameters on the saturation magnetization. The Rechtschaffner design demonstrates that annealing temperature, deposition time and reactional medium temperature are the most influential parameters. Doehlert matrix has been used to predict the optimal condition of the saturation magnetization. XRD data confirm the formation of the desired CoFe_2O_4 phase. SEM analysis reveals the formation of three-dimensional nanoflowers like-morphology. The CV curve of 3D- CoFe_2O_4 nanoflowers thin film deviate from the perfect rectangular shape, demonstrate this pseudocapacitive characteristics. The specific capacitance was found to be 472 F.g^{-1} at 5 mA.s^{-1} scan rate. The VSM measurement demonstrate that the film exhibits a ferrimagnetic behavior, with easy magnetization axis along the plane of the films. The 3D- CoFe_2O_4 elaborated at the optimal conditions shows a maximum saturation magnetization of 0.44 T.

1. Introduction

In recent years, synthesis of magnetic materials with spinel ferrite structure AFe_2O_4 (where A designates a divalent metal ion) [1] has been in the forefront of nanoscience and nanotechnology. These magnetic materials have stimulated the attention of many research group due to their interesting properties in catalysis [2], biosensors [3], biomedical drug delivery [4,5,6], biomolecular separation [7], biocompatible magnetic materials for cancer treatment [8], high density magnetic recording [9] etc, and their excellent magnetodielectric properties [10,11]. Among these magnetic materials, cobalt ferrite CoFe_2O_4 is a semiconductor material with indirect and direct energy band gaps of 1.18 and 2.74 eV respectively [12]. Cobalt ferrite material has an inverse spinel structure with $Fd\bar{3}m$ [1] space group. High coercivity ($\sim 0.43 \text{ T}$) [13], hard magnetic properties, room temperature ferrimagnetism [14], good chemical stability [15], moderate saturation magnetization [16], and excellent electrochemical stability [17] make cobalt ferrites in their different forms interesting material for several technological application. Subsequently, CoFe_2O_4 has been industrially utilized in microwave magnetic devices [18], in biological and spintronic applications [19]. To date, various CoFe_2O_4 morphologies have been reported in literature, such as 1D-nanotube [20], 1D-mesoporous nanowire arrays [21], 1D-nanofibre [22], 2D-nanflakes [23], 2D-porous nanosheets [24,25] and 3D-nanoshpere [26]. Moreover, some research groups have reported that the magnetic properties of CoFe_2O_4 thin films can be affected by many factors like microstructure, grain size, chemical composition, choice of substrate and processing method [27-30] etc.

Note also that different physical and chemical techniques have been used to synthesize CoFe_2O_4 thin films, such as pulsed laser deposition (PLD) [31], molecular beam epitaxy (MBE) [29], RF magnetron sputtering [32], sol-gel [33], chemical bath deposition (CBD) [34], successive ionic layer adsorption and reaction (SILAR) [35] and Spray pyrolysis [19], citrate sol-gel method [36,37] and pulsed electrodeposition [38,39]. Among these methods, chemical bath deposition (CBD) can be classed as the best in terms of simplicity [40], economical, low temperature deposition ($<100 \text{ }^\circ\text{C}$) which avoids oxidation and corrosion of metallic substrates [41] etc. CBD method can offer enhanced control over film thickness, elemental composition, homogeneity, grain structural and film morphology. Thus, CBD is a soft chemical process suited for processing large-area thin films that

allows the control of the preparative parameters such as precursor concentration, deposition time, bath temperature, pH, etc.

Herein we report the preparation of Three-dimensional (3D) CoFe_2O_4 nanoflowers thin films by low-cost chemical bath deposition (CBD) process on stainless steel (SS) substrate. Saturation magnetization is very important factor to determining the heating effect in the treatment of cancer by magnetic hyperthermia. However, this factor has become the subject of experimental modelling. The Rechtschaffner design has been applied to investigate the influence of the principal experimental parameters: temperature deposition (T_d), time deposition (t_d), $R' = [\text{Fe}]/[\text{OH}^-]$ parameter, pH, annealing temperature (T_R) and annealing time (t_R) on the saturation magnetization (M_s). Thereafter, the optimal conditions for the deposition of 3D- CoFe_2O_4 nanoflowers thin films have been studied using Doehlert matrix. The structural properties of the obtained thin film into the optimal conditions have been examined by X-ray diffraction technique. Scanning electron microscopy (SEM), cyclic voltammetry (CV) and vibrating sample magnetometer (VSM) have been used to study the morphological, electrochemical and magnetic properties respectively.

Experimental:

Series of 3D- CoFe_2O_4 nanoflowers thin films have been deposited on 20 mm × 7 mm × 0.15 mm stainless steel (SS) substrates using low-cost chemical bath deposition (CBD) process. In order, to avoid the magnetic contribution of the SS substrates a not-magnetic stainless steel was used AISI 304 L purchased from Goodfellow Cambridge Limited. Before deposition, the stainless steel (SS) substrates were polished using zero fine grade polish paper to remove unwanted oxides formed on the surface. Then, it is cleaned with detergent solution and water. After that substrates have been etched with 2% dilute HCl for 20 s, to remove the surface oxides completely. Finally, substrates have been ultrasonically cleaned with deionized water and dried in air.

All the chemical precursors used in this work were purchased from Aldrich and used without further purification. The bath consists of appropriate amount of 0.2 M iron chloride and 0.1 M of cobalt chloride. The ammonium hydroxide (28%) NH_4OH solution has been added to the prepared solution in order to obtain a basic pH solution. Thereafter, cleaned stainless steel (SS) substrates were immersed in the solution. The bath has been heated during deposition with constant stirring. After few minutes, precipitation has been started, and heterogeneous reaction occurred allowing the formation of hydroxide onto stainless steel (SS) substrates. After deposition, the film has been taken out from the bath and thoroughly washed with de-ionized water and then dried under hot air. Finally, the films have been annealed in air atmosphere to obtain the cubic spinel phase.

The structural characterization has been performed at room temperature using BRUKER diffractometer with Cu – $\text{K}\alpha$ target ($\lambda = 1.5406 \text{ \AA}$). The surface morphology of the 3D- CoFe_2O_4 nanoflowers thin film has been studied by Merlin scanning electron microscopy (SEM) equipped with Silicon Drift Detector (SDD)-X-Max 50 from Oxford Instrument. The electrochemical properties have been performed at room temperature using PGZ-402 potentiostat with a three-electrode cell. The magnetic measurements of the prepared thin films have been recorded by Vibrating Sample Magnetometer (VSM) at room temperature with maximum applied field of $\pm 1500 \text{ kA/m}$.

The active mass of the 3D-CoFe₂O₄ nanoflowers thin films is calculated by double weight method, using the relation:

$$m_A = m_1 - m_2 \quad (1)$$

were:

- m₁: is the mass of substrate without deposit,
- m₂: is the mass after film deposit.

The thickness of the 3D-CoFe₂O₄ nanoflowers thin films was determined by the following relation:

$$e = \frac{m}{S \times \rho} \quad (2)$$

were:

- m is the weight of film,
- S the area of the film
- ρ is the density of CoFe₂O₄.

2. Results and Discussion:

2.1. Influence of the operating parameters on saturation magnetization (M_s) of 3D-CoFe₂O₄ nanoflowers thin films using Rechtschaffner design:

Herein, we seek to investigate the influence of the operating parameters on saturation magnetization of 3D-CoFe₂O₄ nanoflowers thin films. Six main parameters (factors) were chosen: temperature of reactional medium (U₁), deposition time (U₂), concentration ratio R'=[Fe]/[OH⁻] (U₃), pH (U₄), annealing temperature (U₅) and annealing time (U₆). A fractional factorial design 2^{k-1} proposed by Rechtschaffner was carried out to determine the influence of these six factors and their interaction on the 3D-CoFe₂O₄ nanoflowers thin films saturation magnetization. In these types of designs, main effects and two-factor interactions can be estimated, while three factor or more order interactions are negligible [42]. Using Rechtschaffner design, the variables (k) are set at two levels (minimum) and (maximum) normalized as (-1) and (+1).

The experimental response (saturation magnetization (M_s)) associated to the Rechtschaffner design (2⁶⁻¹) was represented by a linear polynomial model given by the following equation:

$$Y = b_0 + b_1X_1 + b_2X_2 + b_3X_3 + b_4X_4 + b_5X_5 + b_6X_6 + b_{12}X_1X_2 + b_{13}X_1X_3 + b_{23}X_2X_3 + b_{14}X_1X_4 + b_{24}X_2X_4 + b_{34}X_3X_4 + b_{15}X_1X_5 + b_{25}X_2X_5 + b_{35}X_3X_5 + b_{45}X_4X_5 + b_{16}X_1X_6 + b_{26}X_2X_6 + b_{36}X_3X_6 + b_{46}X_4X_6 + b_{56}X_5X_6 \quad (3)$$

were

- Y: experimental response (saturation magnetization (M_s))
- X_i: coded variable (-1 or +1)
- b_i: estimation of the principal effect of the factor i for the response Y
- b_{ij}: estimation of interaction effect between factor i and j for the response Y.

Table.1 illustrated the investigated experimental domain. The experimental design and the measured responses are summarized in *Table.2*.

Table.1. Experimental domain investigated for 3D-CoFe₂O₄ nanoflower thin films.

Coded variables (X _i)	Factors (U _i)	Unit	Experimental field	
			Lower limit	Upper limit
X ₁	U ₁ : temperature of reactional medium (T _d)	°C	40	70
X ₂	U ₂ : deposition time (t _d)	min	60	180
X ₃	U ₃ : concentration ratio R' = [Fe]/[OH ⁻]	-	1.11	1.75
X ₄	U ₄ : pH	-	9	10
X ₅	U ₅ : annealing temperature (T _R)	°C	550	750
X ₆	U ₆ : annealing time (t _R)	h	4.30	6

According to the obtained results, the coefficients of the linear polynomial model (eq (3)) are calculated using only extremes by NEMROD Software program (L.P.R.A.I., Marseille, France) [43,44]:

$$Y = 149.988 + 12.044 X_1 + 23.426 X_2 - 7.910 X_3 - 0.597 X_4 + 49.285 X_5 - 7.490 X_6 + 25.575 X_1X_2 - 3.264 X_1X_3 - 3.269 X_2X_3 - 3.756 X_1X_4 - 10.869 X_2X_4 - 6.285 X_3X_4 + 11.577 X_1X_5 + 27.019 X_2X_5 + 8.733 X_3X_5 - 1.557 X_4X_5 + 3.422 X_1X_6 + 5.237 X_2X_6 - 9.505 X_3X_6 - 7.412 X_4X_6 + 1.386 X_5X_6 \quad (4)$$

The effects and interactions of the different investigated factors are shown in *Fig.1. a*. As can be seen the saturation magnetization is very influenced by the annealing temperature as it has a positive effect on the studied response. In fact, the increasing of annealing temperature leads to increase the saturation magnetization. In addition, the reactional medium temperature and deposition time are the second most significant factors that have positive effect on the studied response. Thus, in order to improve the saturation magnetization, it will be useful to increase the reactional medium temperature and deposition time. On the other hand, the coefficient associated with the interaction term (X₁X₂) that has a positive effect on the studied response, has a very important value. Thereby, for the experimental domain investigated, the effect of X₁ factor (temperature of reactional medium) depend on the level of X₂ factor (deposition time). Note also that the effects of the other factors are very negligible.

Table.2. Rechtschaffner experimental design 2^{6-1} , experimental plan and results.

Experimental number	Experimental design						Experimental plan						Results Y (T)
	X ₁	X ₂	X ₃	X ₄	X ₅	X ₆	U ₁	U ₂	U ₃	U ₄	U ₅	U ₆	
1	-1	-1	-1	-1	-1	-1	40	60	1.11	9	550	4.30	0.029
2	-1	1	1	1	1	1	40	180	1.75	10	750	6	0.05
3	1	-1	1	1	1	1	70	60	1.75	10	750	6	0.04
4	1	1	-1	1	1	1	70	180	1.11	10	750	6	0.091
5	1	1	1	-1	1	1	70	180	1.75	9	750	6	0.1
6	1	1	1	1	-1	1	70	180	1.75	10	550	6	0.028
7	1	1	1	1	1	-1	70	180	1.75	10	750	4.30	0.088
8	1	1	-1	-1	-1	-1	70	180	1.11	9	550	4.30	0.04
9	1	-1	1	-1	-1	-1	70	60	1.75	9	550	4.30	0.021
10	1	-1	-1	1	-1	-1	70	60	1.11	10	550	4.30	0.039
11	1	-1	-1	-1	1	-1	70	60	1.11	9	750	4.30	0.041
12	1	-1	-1	-1	-1	1	70	60	1.11	9	550	6	0.026
13	-1	1	1	-1	-1	-1	40	180	1.75	9	550	4.30	0.025
14	-1	1	-1	1	-1	-1	40	180	1.11	10	550	4.30	0.03
15	-1	1	-1	-1	1	-1	40	180	1.11	9	750	4.30	0.051
16	-1	1	-1	-1	-1	1	40	180	1.11	9	550	6	0.031
17	-1	-1	1	1	-1	-1	40	60	1.75	10	550	4.30	0.049
18	-1	-1	1	-1	1	-1	40	60	1.75	9	750	4.30	0.051
19	-1	-1	1	-1	-1	1	40	60	1.75	9	550	6	0.026
20	-1	-1	-1	1	1	-1	40	60	1.11	10	750	4.30	0.056
21	-1	-1	-1	1	-1	1	40	60	1.11	10	550	6	0.047
22	-1	-1	-1	-1	1	1	40	60	1.11	9	750	6	0.041

Pareto analysis allows to check the weight of different coefficients in the experimental domain investigated [45,46]. In fact, the advantage of this analysis is that the numerical values of each effects are displayed. Thus, this analysis calculates the percentage effect of each factor on the response investigated using the relation (5) [46]:

$$P_i = \left(\frac{b_i^2}{\sum b_i^2} \right) \times 100 \quad (i \neq 0) \quad (5)$$

Fig.1.b shows a typical Pareto graphic analysis. As can be seen in this figure, the annealing temperature is the most influential factors on the saturation magnetization. His total contribution on the investigated response reach 46.7 %. On the other hand, the temperature of reactional medium and deposition time have total contribution on the saturation magnetization of the order of 11.9 and 5.1 % respectively. Furthermore, these factors have an important and meaningful positive interaction with a contribution of 12.9 %. Thus, we can note that more than 75 % of the response are bringing by these three factors and their interactions. Moreover, the pH, R', annealing time and their interactions have a negligible effect with only 15 % of the response.

Thereby, in order to increase the saturation magnetization, R' factor and the annealing time were fixed at the lowest values, 1.75 and 4h30 respectively, while the pH was fixed at the highest value (pH = 10).

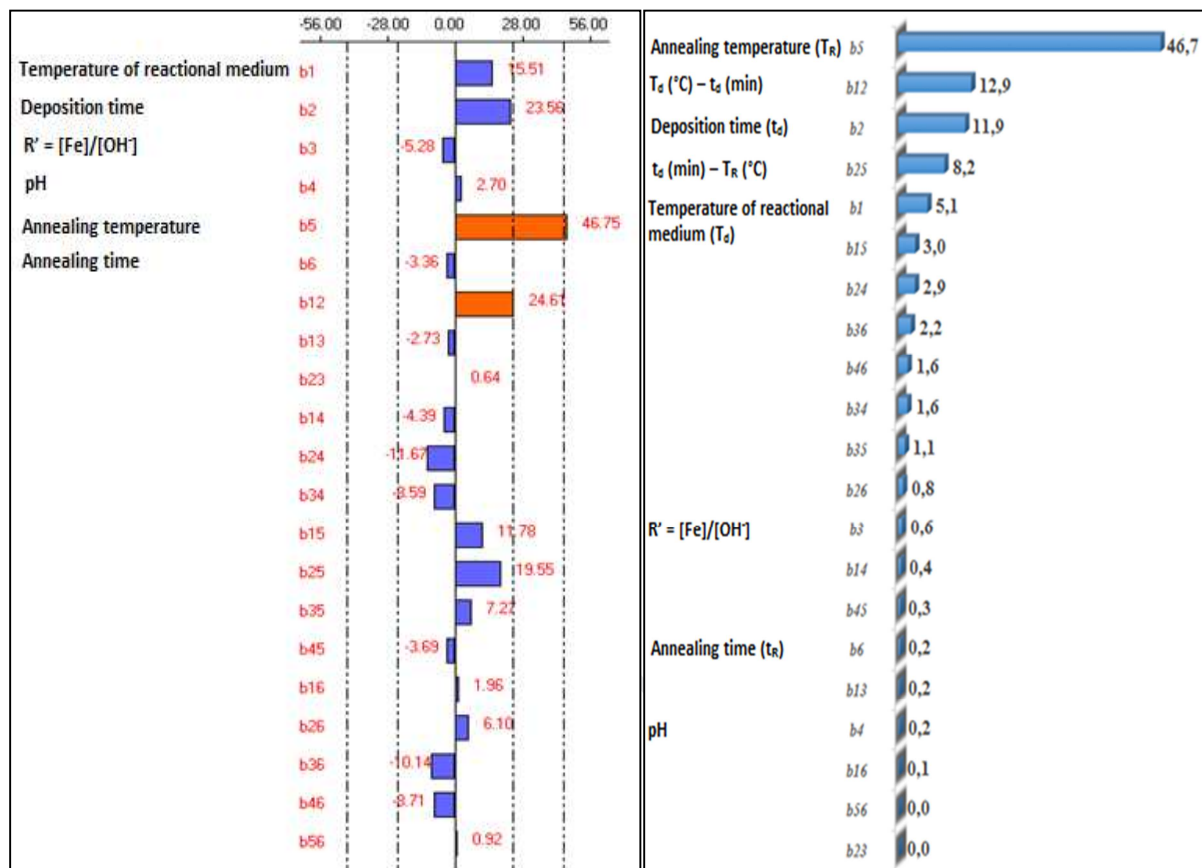


Fig.1. (a) Graphical analysis of the effect of: temperature of reactional medium, deposition time, R' , pH, annealing temperature and annealing time, (b) Graphical Pareto analysis.

2.2. Determination of the optimal condition using Doehlert design

The approach of Doehlert [45-47] was applied in order to determine the optimal condition that allowed the formation of homogenous 3D- $CoFe_2O_4$ nanoflowers thin films with maximum saturation magnetization. Based on the last study, three factors such as the temperature of reactional medium, deposition time and annealing temperature will be studied. Indeed, the approach of Doehlert is formed by uniformly distributed of the experimental points within the space filling of the coded variables (X_i). In addition, the advantages of this approach are the ability to explore the total experimental domain through a minimum number of experiments as well as to extend the domain by adding another factor [47].

As mentioned in the above discussion, three main factors were studied in the investigated field: reactional medium temperature, deposition time and annealing temperature. In order to compare the effects of the three factors U_i cited previously in the experimental domain (Table.3), concerned coded variables were used. However, these factors were correlated to resolve and reach the optimal condition, where:

U_1 : is the first factor corresponding to the deposition time $\{t_d \text{ (min)}\}$,

U_2 : is the second factor corresponding to the annealing temperature $\{T_R \text{ (}^\circ\text{C)}\}$,

U_3 : is the third factor corresponding to the reactional medium temperature $\{T_d \text{ (}^\circ\text{C)}\}$.

For calculation, the experimental value of the factors U_1 , U_2 and U_3 were transformed into coded X_1 , X_2 and X_3 using the following relation:

$$X_i = \frac{U_i - \bar{U}_i}{\Delta U_i} \quad (6)$$

$$\bar{U}_i = \frac{\text{upper limit of } (U_i) + \text{lower limit of } (U_i)}{2} \quad (7)$$

$$\Delta U_i = \frac{\text{upper limit of } (U_i) - \text{lower limit of } (U_i)}{2\gamma_i} \quad (8)$$

Where γ_i is the coded value limit for each factor: $\gamma_1 = 1$; $\gamma_2 = 0.866$; $\gamma_3 = 0.816$.

The experimental response (saturation magnetization (M_s)) associated to the Doehlert approach can be described as following by a second-degree quadratic polynomial equation:

$$Y = b_0 + b_1X_1 + b_2X_2 + b_3X_3 + b_{11}X_1^2 + b_{22}X_2^2 + b_{33}X_3^2 + b_{12}X_1X_2 + b_{13}X_1X_3 + b_{23}X_2X_3 \quad (9)$$

Where:

Y : the experimental response (saturation magnetization);

b_0 : an independent term;

b_i : the coefficients of the linear terms;

b_{ii} : the coefficients of the quadratic terms;

b_{ij} : the coefficients corresponding to the interaction term between the factor i and the factor j .

Table.3. Experimental domain investigated for 3D-CoFe₂O₄ nanoflower thin films.

Coded variables (X_i)	Factors	Unit	Experimental domain	
			Lower limit	Upper limit
X_1	U_1 : deposition time	min	60	180
X_2	U_2 : annealing temperature	$^\circ\text{C}$	550	750
X_3	U_3 : temperature of reactional medium	$^\circ\text{C}$	40	70

In addition, the calculation of the coefficients of this model was carried through the least squares method:

$$B = (X^T X)^{-1} \times X^T \times Y \quad (10)$$

Where: B is the estimates coefficients vector; X^T is the transposed model matrix; X is the model matrix and Y is the measured response vector. Using Doehlert approach, the number of experiments (N) required is given by the following relation: $N = k + k^2 + 1$, where k is the number of factors. For the three factors previously mentioned ($k = 3$), 13 different experiments were required. However, in order to validate this model, three replicated experiments at the center level were carried out. Doehlert matrix, experimental plan and results for the three selected factors were listed in [Table.4](#).

Based to these results, the coefficients of the polynomial model were calculated using NEMROD Software program:

$$Y = 211.02 + 29.29 X_1 + 87 X_2 - 43.99 X_3 - 72.54 X_1^2 + 19.88 X_2^2 - 46.19 X_3^2 + 62.62 X_1 X_2 - 35.19 X_1 X_3 - 65.79 X_2 X_3 \quad (11)$$

Table.4. Doehlert matrix experiments and experimental results (Y)

Experiment number	Doehlert matrix			Experimental plan			Y (T)
	X ₁	X ₂	X ₃	U ₁	U ₂	U ₃	
1	1.0000	0.0000	0.0000	180	650	55	0.05
2	-1.0000	0.0000	0.0000	60	650	55	0.036
3	0.5000	0.8660	0.0000	150	750	55	0.1
4	-0.5000	-0.8660	0.0000	90	550	55	0.04
5	0.5000	-0.8660	0.0000	150	550	55	0.045
6	-0.5000	0.8660	0.0000	90	750	55	0.067
7	0.5000	0.2887	0.8165	150	683	70	0.043
8	-0.5000	-0.2887	-0.8165	90	617	40	0.046
9	0.5000	-0.2887	-0.8165	150	617	40	0.05
10	0.0000	0.5774	-0.8165	120	716	40	0.098
11	-0.5000	0.2887	0.8165	90	683	70	0.046
12	0.0000	-0.5774	0.8165	120	584	70	0.038
13	0.0000	0.0000	0.0000	120	650	55	0.066
14	0.0000	0.0000	0.0000	120	650	55	0.066
15	0.0000	0.0000	0.0000	120	650	55	0.065

In order to interpret well the effect of different factors interactions on the saturation magnetization (M_s), the typical contour plots and the three-dimensional response representations versus deposition time, annealing temperature and reactional medium temperature were shown in [Figs.2-4](#).

The effects of interaction between deposition time and annealing temperature on saturation magnetization were represented in [Fig.2](#) at a fixed temperature of reactional medium of 55 °C. As can be seen, the maximums of saturation magnetization are obtained when annealing temperature tend towards 750 °C. In addition, it is found that the extension of the deposition time and of the annealing temperature (≥ 650 °C) entails an increase in the investigated response. On the other hand, the analysis of the isoresponse curves at a fixed deposition time of 120 min ([Fig.3](#)) shows that the increase in temperature of reaction medium for annealing temperatures ≤ 650 °C entails a decrease in the saturation magnetization. The obtained result confirms the value observed for the interaction between the temperature of reaction medium and annealing temperature ($b_{12} = -65.79$). In fact, this interaction presents a negative effect on the studied response. Regardless the deposition time, the increase of the temperature of reaction medium to values higher than 55 °C causes a decrease in the saturation magnetization ([Fig.4](#)). Indeed, the film saturation magnetization (M_s) reaches their maximum values when deposition time range between 120 and 150 min, and when temperature of reaction medium range between 40 and 55 °C. Consequently, the optimal working condition that allows the formation of 3D-CoFe₂O₄ nanoflowers thin film with 0.44 T saturation magnetization was found to be as following: $t_d = 146$ min, $T_R = 750$ °C and $T_d = 51$ °C.

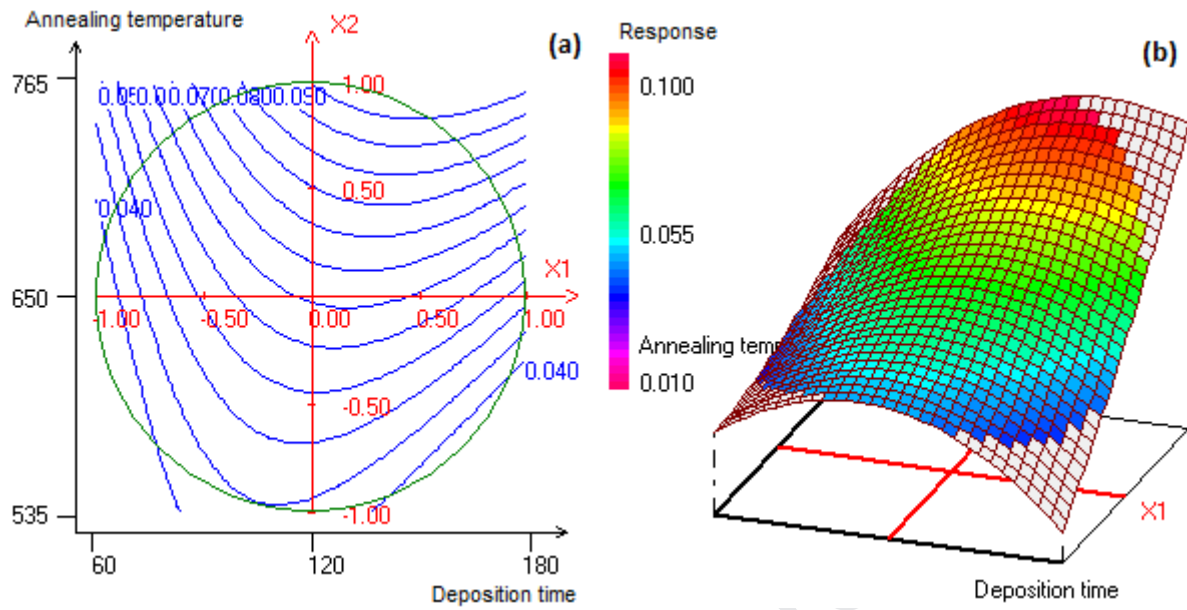


Fig.2. (a) Contour plots of saturation magnetization (M_s) versus annealing temperature (°C) and deposition time (min) at fixed reactional medium temperature (55 °C); (b) The corresponding three-dimensional plot.

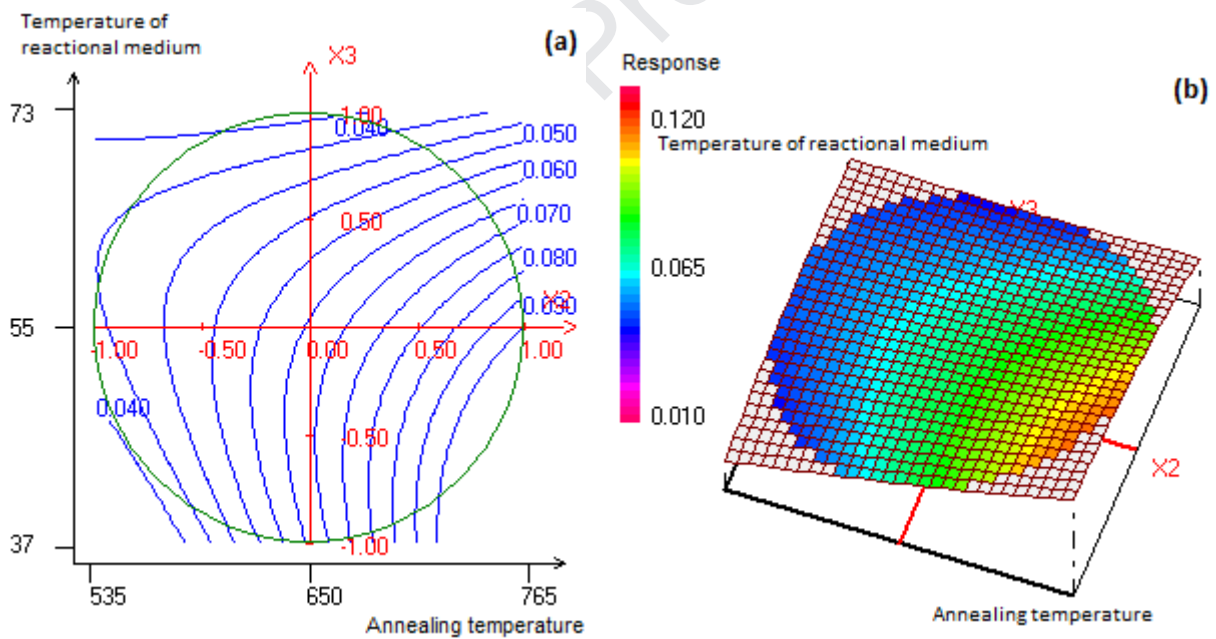


Fig.3. (a) Contour plots of saturation magnetization (M_s) versus temperature of reactional medium (°C) and annealing temperature (°C) at fixed deposition time (120 min); (b) The corresponding three-dimensional plot.

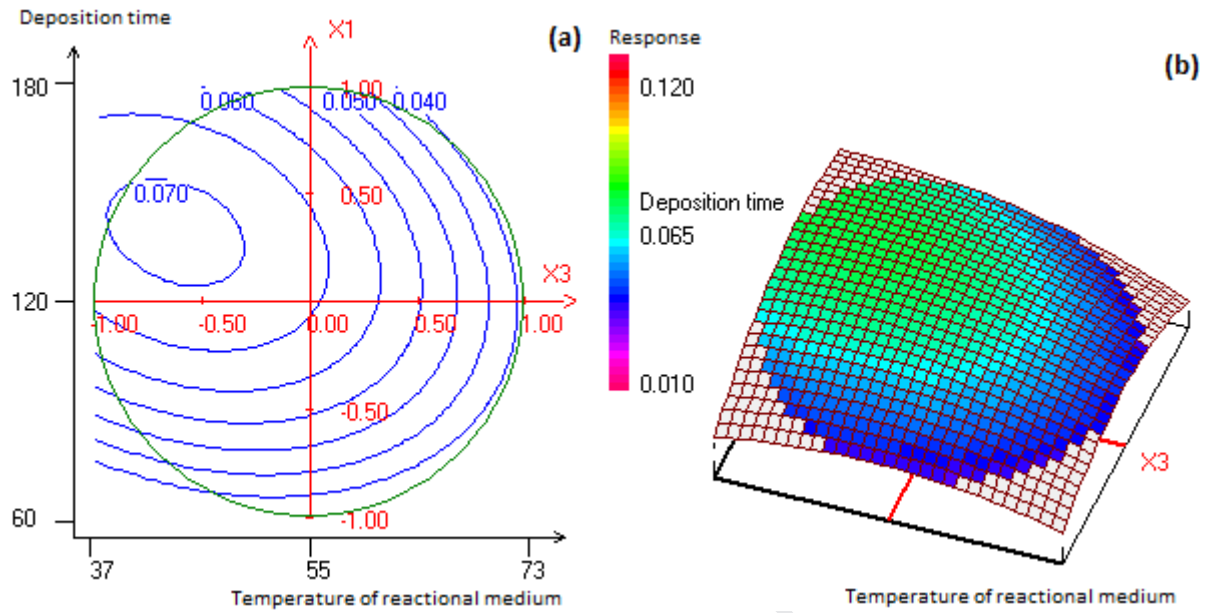


Fig.4. (a) Contour plots of saturation magnetization (M_s) versus deposition time (min) and temperature of reactional medium ($^{\circ}\text{C}$) at fixed annealing temperature ($650\text{ }^{\circ}\text{C}$); (b) The corresponding three-dimensional plot.

3. Characterization of 3D- CoFe_2O_4 nanoflowers thin film obtained based on the optimal condition

3.1. Structural analysis

Fig.5 depicts the X-Ray diffraction pattern of 3D- CoFe_2O_4 nanoflowers thin film deposited under the optimal condition determined from Doehlert matrix ($t_d = 146\text{ min}$, $T_R = 750\text{ }^{\circ}\text{C}$ at $T_d = 51\text{ }^{\circ}\text{C}$). According to the crystallographic data of the obtained X-ray diffractogramme (Fig.5) and based to the joint committee powder diffraction standards (JCPDS) data (PDF N $^{\circ}$ 22-1086), we can confirm the formation of the spinel ferrite structure CoFe_2O_4 that crystallizes in cubic symmetry with $\text{Fd}\bar{3}\text{m}$ space group. Were related to thus, the observed reflection peaks located at 30.13° ; 35.45° ; 44.49° ; 57.04° ; 74.93° were assigned to the (2 2 0); (3 1 1); (4 0 0); (5 1 1) and (5 3 3) planes respectively. Whereas, peaks located at 43.59° , 50.86° and 74.68° were attributed to stainless steel (SS) substrate. Note also that this pattern shows very broad diffraction peaks that indicates the ultra-fine nature of the obtained film.

Debye Scherrer's [47] formula was used to determine the crystallite size (D_s) of 3D- CoFe_2O_4 nanoflowers thin film using the full width at half maximum (FWHM) of the most intense reflection peak (311):

$$D_s = \frac{k\lambda}{\beta \cos(\theta)} \quad (12)$$

where D_s is the crystallite size, λ is the wavelength of Cu (K_{α}), k is the Scherer's constant (0.90), β is the full width at half maximum (FWHM) and θ is the Bragg's diffraction angle. Indeed, $\beta^2 = (\beta_M^2 - \beta_S^2)$, where β_M is the full width at half maximum (FWHM) of the most intense peak (311) and β_S is the standard instrumental broadening (0.0480°).

The lattice strain (ϵ) of the deposited 3D-CoFe₂O₄ nanoflowers thin film was determined by the following formula [47]:

$$\epsilon = \frac{\beta \times \cos \theta}{4} \quad (13)$$

where ϵ is the lattice strain, β is the full width at half maximum (FWHM) and θ is the Bragg angle.

The crystallite size (D_c) and lattice strain (ϵ) determined from the above formulas were found to be in the order of 313 nm and 0.423 respectively. It is well known that the electrical and magnetic parameters for the complex oxides strongly depend on the average and distribution of crystallite size [48,49].

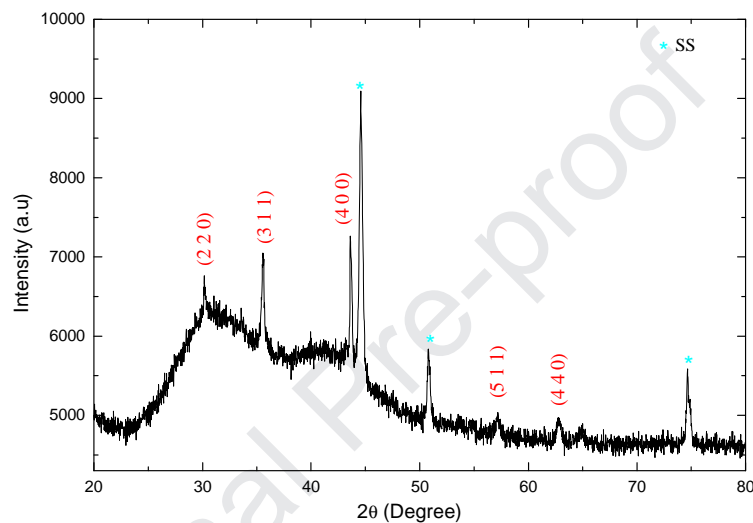


Fig.5. X-ray diffraction pattern of 3D-CoFe₂O₄ nanoflowers thin film deposited at $t_d = 146$ min, $T_R = 750$ °C and $T_d = 51$ °C.

3.2. Morphological properties

In order to further study the properties of the obtained 3D-CoFe₂O₄ nanoflowers thin film deposited under the optimal condition, their size and morphology nature were determined. Fig.6 a-c shows the SEM micrographs of 3D-CoFe₂O₄ nanoflowers thin film grown at $t_d = 146$ min, $T_R = 750$ °C and $T_d = 51$ °C. Fig.6a revealed that the obtained CoFe₂O₄ thin film was formed by nanoflowers like morphology with regular and irregular shapes. It can be seen also that these nanoflowers are formed by the agglomerated nanosheets, with thickness range between 6.69 and 57.63 nm (Fig.6b). These nanosheets are interconnected with each other forming an array of nanoflowers with porous structure. Additionally, the pores size of our nanosheets surface was found in the range of 19.49 - 95.53 nm (Fig.6c). The porous surface of the nanosheets improve the performance of the CoFe₂O₄ thin films in supercapacitor application. The energy dispersive X-ray spectrometry (EDS) of the obtained 3D-CoFe₂O₄ nanoflowers thin film was illustrated in Fig.6d. The EDS spectra shows that the Fe/Co and O/Co atomic percentage ratios equal to 2.05 % and 4.2 % respectively. This stoichiometric ratio confirms the formation of stoichiometric ferrite cobalt thin film with oxygen excess. The absence of other elements indicates the high purity of the 3D-CoFe₂O₄ nanoflowers thin film. In our Knowledge, the complex 3d-metal oxides easily allow the oxygen excess and deficit. However,

oxygen excess and deficit can increase or decrease the oxidation degree of 3d-metals and changing magnetic and electrical parameters [50,51]. Moreover, oxygen vacancies effect on exchange interactions. In complex oxides, there is only indirect exchange according to Goodenough-Kanamori empirical rules [52,53].

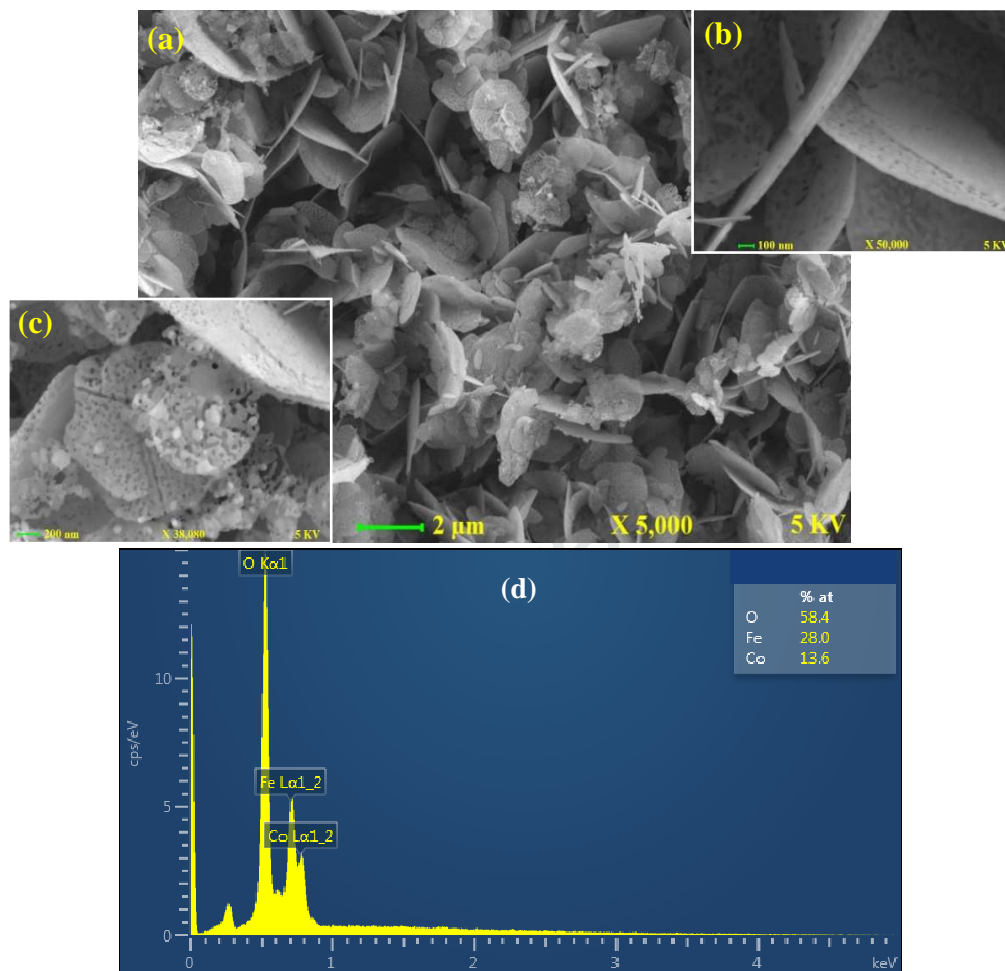


Fig.6. SEM micrographs of 3D-CoFe₂O₄ nanoflowers thin film grown at $t_d = 146$ min, $T_R = 750$ °C and $T_d = 51$ °C with 5.000 X magnification (a), estimated nanosheets thickness (b) and estimated pores size (c).

3.3. Electrochemical properties

The electrochemical performance of 3D-CoFe₂O₄ nanoflowers thin film prepared under optimal conditions was carried out by constructing a cell with three electrodes configuration in 1M NaOH electrolyte. The electrochemical cell was consisted by our 3D-CoFe₂O₄ nanoflowers thin film as a working electrode, mercury-mercury oxide (Hg/HgO) as reference electrode and stainless steel (SS) wire as counter electrode. The active mass and thickness of the 3D-CoFe₂O₄ nanoflowers thin film obtained are equal to 3.8 mg and 6.8 μm respectively. Fig.7 depicts the obtained cyclic voltammetry (CV) curve at scan rate of 20 mV.s⁻¹ and within the negative potential window of -1.2 to 00 V. Notably, the CV curve of 3D-CoFe₂O₄ nanoflowers thin film deviate from the perfect rectangular shape. Additionally, the CV curve exhibit an anodic peak occurs nearly to -0.98 V and a cathodic peak at around -0.62 V. These peaks can be associated to the reversible electrochemical reactions (M-

O/M-OOH, where M: Fe or Co), which demonstrates the pseudocapacitive contribution of the 3D-CoFe₂O₄ nanoflowers thin film to the electrochemical performances.

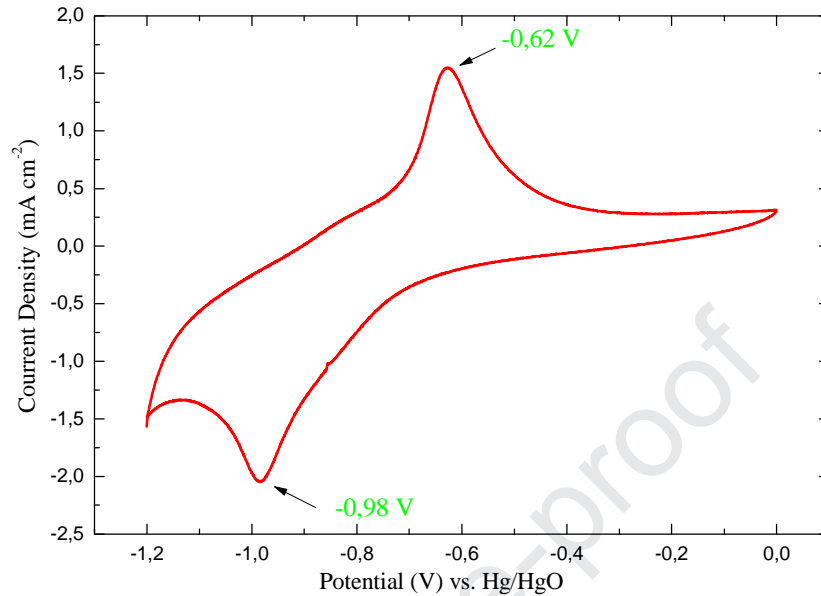


Fig.7. Cyclic voltammogram of 3D-CoFe₂O₄ nanoflowers thin film in 1M NaOH electrolyte, at 20 mV.s⁻¹ and within the potential window of -1.2 to 0.0 V.

In order to evaluate the scan rate on stability of the 3D-CoFe₂O₄ thin film, the cyclic voltammograms (CV) test is performed with a wide scan range that extend from 5 to 100 mV.s⁻¹. To the best of our knowledge, the encircled area of CV curves is proportional to the specific capacitance C_s of the CoFe₂O₄ electrode. However, the specific capacitance (C_s) is calculated from the CV curves using the following relation [54]:

$$C_s = \frac{\int_{V_1}^{V_2} i \times dV}{m \times v \times (V_2 - V_1)} \quad (14)$$

where C_s is the specific capacitance (F.g⁻¹), V_1 and V_2 are the two working potential limits (V), i is the corresponding current (mA.cm⁻²), m is the active mass of the active material (g) and v is the scan rate (mV.s⁻¹).

Fig.8 displays the CV curves of 3D-CoFe₂O₄ nanoflowers thin film at different scan rates in potential windows range -1.2 - 0.0 V. As shown, regardless the scan rate all the CV curves exhibit a symmetric and identical shape with pair of redox peaks indicating the excellent pseudocapacitive nature of this film. Moreover, when scan rate was increased, the area under the CV curve also increases, while the specific capacitance C_s decreases from 472 to 162 F.g⁻¹ (Insert-Fig.8). At high scan rate, the electrolytic ions access only in outer active sites surface of the electrode, due to the short time of intercalation. Which, decreasing the accessibility of all active materials during the charging stockage mechanism. Otherwise at low scan rates, the electrolytic ions get enough time to access the outer and inner the pore of the porous electrode, which is reflected by an increase in the specific capacitance.

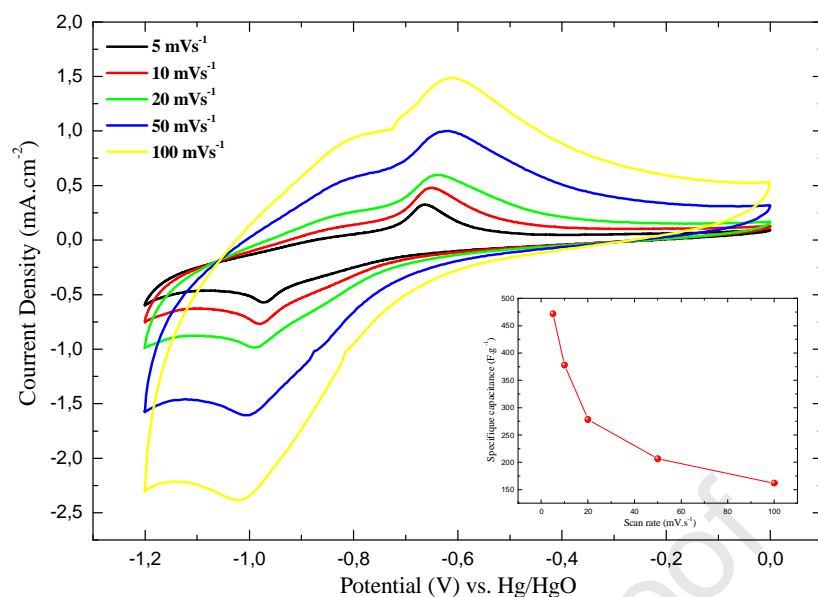


Fig.8. Cyclic voltammetry curves of 3D-CoFe₂O₄ nanoflowers thin film at different scan rates and insert of the specific capacitance variation as a function of scan rate.

3.4. Magnetic properties

Fig.9 shows the magnetic hysteresis loops of 3D-CoFe₂O₄ nanoflowers thin film deposited under the optimal condition in which the magnetic field was measured in and out-of-plane at room temperature. It can be easily observed that the film exhibits a ferrimagnetic behavior at room temperature with a large saturation magnetization. The in-plane saturation magnetization value of the film was found about 0.44 T, whereas the out-of-plane saturation magnetization reaches the maximum value at 0.07 T. However, this significant difference between in-plane and out-of-plane saturation magnetization is due to effect of magnetic anisotropy. Consequently, the 3D-CoFe₂O₄ nanoflowers thin film has an easy magnetization axis along the plane of the film. Similar behavior was detected with an easy-magnetization in-plane, for epitaxial CoFe₂O₄ films grown on SrTiO₃ (001) [55,56] and MgAl₂O₄ [57] (001) substrates. On the contrary, H. Yanagihara et al. [58], and M. Ning et al. [59] shows an easy axis of magnetization perpendicular to the surface plane when cobalt ferrites are grown onto in-plane tensile strain such as MgO substrates [58] or Si buffer with MgO thin films respectively. On the other hand, the coercivity field in-plane and out-of-plane were found to be 6.92 and 12.97 kA/m respectively.

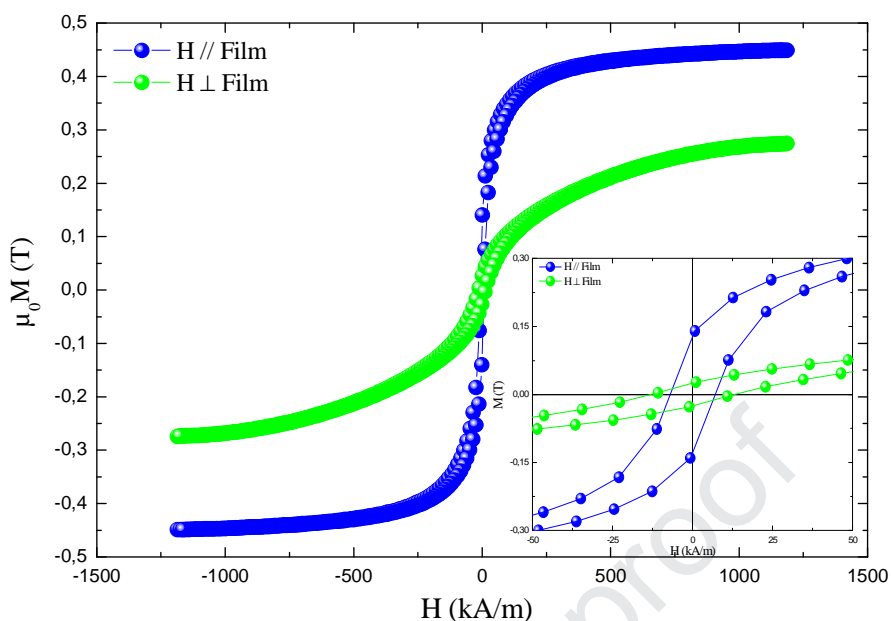


Fig.9. M-H hysteresis loops of the 3D-CoFe₂O₄ nanoflowers thin film with measuring filed parallel and perpendicular to the film surface at 300K.

Conclusion

In summary, Three-dimensional (3D) CoFe₂O₄ nanoflowers thin films were successfully deposited by low-cost chemical bath deposition (CBD) process. In order to study the effect of the six deposition parameters on saturation magnetization, an experimental design methodology was adopted. Firstly, the Rechtschaffner design demonstrates that only the annealing temperature, deposition time and temperature of reactional medium are the most influential parameters. Secondly, based to Doehlert matrix, we have been able to define the optimal working condition for a maximum saturation magnetization. In fact, we have demonstrated that the following conditions: $t_d = 146$ min, $T_R = 750$ °C and $T_d = 51$ °C, lead to saturation magnetization of the order of 0.44 T in-plane of the film. The structural study confirms the formation of well crystallized CoFe₂O₄ film with cubic symmetry and $Fd\bar{3}m$ space group. SEM study revealed that the obtained CoFe₂O₄ thin film has nanoflowers like morphology with regular and irregular shapes. The specific capacitance was found to be 472 F.g⁻¹. Moreover, 3D-CoFe₂O₄ nanoflowers thin film exhibit a pseudocapacitive behavior, which allows to be used as a negative electrode in supercapacitor.

Acknowledgements

This work is mainly supported by Ministry of Higher Education and Scientific Research Tunisia and the French National Center for Scientific Research (CNRS).

References

- [1] N. Hosni, K. Zehani, T. Bartoli, L. Bessais, and H. Maghraoui-Meherzi, Semi-hard magnetic properties of nanoparticles of cobalt ferrite synthesized by the co-precipitation process, *J. Alloys Compd.* 694 (2017) 1295-1301. <https://doi.org/10.1016/j.jallcom.2016.09.252>
- [2] V. Polshettiwar, R. Luque, A. Fihri, H. Zhu, M. Bouhrara, J.M. Basset, Magnetically Recoverable Nanocatalysts, *Chem. Rev.* 111 (2011) 3036-3075. <https://doi.org/10.1021/cr100230z>.
- [3] D. M. Bruls, T. H. Evers, J. A. H. Kahlman, P. J. W. van Lankvelt, M. Ovsyanko, E. G. M. Pelssers, J. J. H. B. Schleipen, F. K. de Theije, C. A. Verschuren, T. van der Wijk, J. B. A. van Zon, W. U. Dittmer, A. H. J. Immink, J. H. Nieuwenhuis and M. W. J. Prins, Rapid integrated biosensor for multiplexed immunoassays based on actuated magnetic nanoparticles, *Lab Chip.* 9 (2009) 3504–3510. <https://doi.org/10.1039/B913960E>.
- [4] C. Sun, J. S. H. Lee, M. Zhang, Magnetic nanoparticles in MR imaging and drug delivery, *Adv. Drug Delivery Rev.* 60 (2008) 1252-1265. <https://doi.org/10.1016/j.addr.2008.03.018>.
- [5] K. Dukenbayev, I.V. Korolkov, D.I. Tishkevich, A.L. Kozlovskiy, S.V. Trukhanov, Y.G. Gorin, E.E. Shumskaya, E.Y. Kaniukov, D.A. Vinnik, M.V. Zdorovets, M. Anisovich, A.V. Trukhanov, D. Tosi, C. Molardi, Fe₃O₄ nanoparticles for complex targeted delivery and boron neutron capture therapy, *Nanomaterials-Basel* 9 (2019) 494. <https://doi.org/10.3390/nano9040494>.
- [6] D.I. Tishkevich, I.V. Korolkov, A.L. Kozlovskiy, M. Anisovich, D.A. Vinnik, A.E. Ermekova, A.I. Vorobjova, E.E. Shumskaya, T.I. Zubar, S.V. Trukhanov, M.V. Zdorovets, A.V. Trukhanov, Immobilization of boron-rich compound on Fe₃O₄ nanoparticles: Stability and cytotoxicity, *J. Alloys Compd.* 797 (2019) 573-581. <https://doi.org/10.1016/j.jallcom.2019.05.075>.
- [7] C. Scherer, A. M. Figueiredo Neto, Ferrofluids: properties and applications, *Braz. J. Phys.* 35 (2005) 718-727. <http://dx.doi.org/10.1590/S0103-97332005000400018>.
- [8] L. Kumar, P. Kumar, M. Kar, Effect of non-magnetic substitution on the structural and magnetic properties of spinel cobalt ferrite ceramics, *J. Mater. Sci: Mater. electron.* 24 (2013) 2706-2715. <https://doi.org/10.1021/acs.chemmater.5b01034>.
- [9] D. H. Kim, D. E. Nikles, D. T. Johnson, C. S. Brazel, Heat generation of aqueously dispersed CoFe₂O₄ nanoparticles as heating agents for magnetically activated drug delivery and hyperthermia. *J. Magn. Mater.* 320 (2008) 2390– 2396. <https://doi.org/10.1016/j.jmmm.2008.05.023>.
- [10] M.A. Almessiere, A.V. Trukhanov, F.A. Khan, Y. Slimani, N. Tashkandi, V.A. Turchenko, T.I. Zubar, D.I. Tishkevich, S.V. Trukhanov, L.V. Panina, A. Baykal, Correlation between microstructure parameters and anti-cancer activity of the [Mn_{0.5}Zn_{0.5}](EuxNd_xFe_{2-2x})O₄ nanoferrites produced by modified sol-gel and ultrasonic methods, *Ceram. Int.* 46 (2020) 7346-7354. <https://doi.org/10.1016/j.ceramint.2019.11.230>.

- [11] M.A. Almessiere, Y. Slimani, H. Güngüneş, V.G. Kostishyn, S.V. Trukhanov, A.V. Trukhanov, A. Baykal, Impact of Eu³⁺ ion substitution on structural, magnetic and microwave traits of Ni-Cu-Zn spinel ferrites, *Ceram. Int.* 46 (2020) 11124-11131. <https://doi.org/10.1016/j.ceramint.2020.01.132>.
- [12] B. S. Holinsworth, D. Mazumdar, H. Sims, Q.-C. Sun, M. K. Yurtisigi, S. K. Sarker, A. Gupta, W. H. Butler, and J. L. Musfeldt, Chemical tuning of the optical band gap in spinel ferrites: CoFe₂O₄ vs NiFe₂O₄, *Appl. Phys. Lett.* 103 (2013) 082406. <https://doi.org/10.1063/1.4818315>.
- [13] N. Adeela, U. Khan, S. Naz, K. Khan, R.U.R. Sagar, S. Aslam, D. Wu, Structural and magnetic response of Ni_x substitution in Co_{0.8-x}Mn_{0.2}Fe₂O₄ Spinel Ferrites, *Mater. Res. Bull.* (2018) <https://doi.org/10.1016/j.materresbull.2018.06.032>.
- [14] G. Dascalu, G. Pompilian, B. Chazallon, O. F. Caltun, S. Gurlui, C. Focs, Femtosecond pulsed laser deposition of cobalt ferrite thin films, *Appl. Surf. Sci.* 278 (2013) 38–42. <https://doi.org/10.1016/j.apsusc.2013.02.107>.
- [15] S. N. Okuno, S. Hashimoto, K. Inomata, Preferred crystal orientation of cobalt ferrite thin films induced by ion bombardment during deposition, *J. Appl. Phys.* 71 (1992) 5926. <https://doi.org/10.1063/1.350442>.
- [16] M. Oujja, L. Martín-García, E. Rebollar, A. Quesada, M.A. García, J. F. Fernández, J. F. Marco, J. de la Figuera, M. Castillejo, Effect of wavelength, deposition temperature and substrate type on cobalt ferrite thin films grown by pulsed laser deposition, *Appl. Surf. Sci.* 452 (2018) 19-31. <https://doi.org/10.1016/j.apsusc.2018.05.012>.
- [17] G. Vaidyanathan, S. Sendhilnathan, Characterization of Co_{1-x}Zn_xFe₂O₄ nanoparticles synthesized by co-precipitation method. *Physica B.* 403 (2008) 2157–2167. <https://doi.org/10.1016/j.physb.2007.08.219>.
- [18] I. H. Gul, A. Z. Abbasi, F. Amin, M. Anis-ur-Rehman, A. Maqsood, Structural, magnetic and electrical properties of Co_{1-x}Zn_xFe₂O₄ synthesized by co-precipitation method, *J. Magn. Mater.* 311 (2007) 494-499. <https://doi.org/10.1016/j.jmmm.2006.08.005>.
- [19] M. Penchal Reddy, A. M. A. Mohamed, One-pot solvothermal synthesis and performance of mesoporous magnetic ferrite MFe₂O₄ nanospheres, *Microporous Mesoporous Mater.* 215 (2015) 37-45. <https://doi.org/10.1016/j.micromeso.2015.05.024>.
- [20] X. Zhang, Y. Xie, Y. Sun, Q. Zhang, Q. Zhu, D. Hou, J. Guo, Self-template synthesis of CoFe₂O₄ nanotubes for high-performance lithium storage, *RSC Adv.* 5 (2015) 29837-29841. <https://doi.org/10.1039/C5RA00428D>.
- [21] B. Wang, S. Li, X. Wu, B. Li, J. Liu, M. Yu, Nanocrystal-constructed mesoporous CoFe₂O₄ nanowire arrays aligned on flexible carbon fabric as integrated anodes with enhanced lithium storage properties. *Phys. Chem. Chem. Phys.* 17 (2015) 21476-21484. <https://doi.org/10.1039/C5CP03042K>.
- [22] L. Khalil, C. Eid, M. Bechelany, N. Abboud, A. Khoury, P. Miele, Design of CoFe₂O₄/Co₃O₄ nanofibers with tunable morphology by Electrospinning. *Mater. Lett.* 140 (2015) 27–30. <https://doi.org/10.1016/j.matlet.2014.10.155>.

- [23] V. S. Kumbhar, A. D. Jagdale, N. M. Shinde, C. D. Lokhande, Chemical synthesis of spinel cobalt ferrite (CoFe₂O₄) nano-flakes for supercapacitor application, *Appl. Surf. Sci.* 259 (2012) 39– 43. <https://doi.org/10.1016/j.apsusc.2012.06.034>.
- [24] X. Yao, J. Kong, X. Tang, D. Zhou, C. Zhao, R. Zhou and X. Lu, Facile synthesis of porous CoFe₂O₄ nanosheets for lithium-ion battery anodes with enhanced rate capability and cycling stability, *RSC Adv.* 4 (2014) 27488–27492. <https://doi.org/10.1016/j.pnsc.2016.09.001>.
- [25] H. Gao, J. Xiang, Y. Cao, Hierarchically porous CoFe₂O₄ nanosheets supported on Ni foam with excellent electrochemical properties for asymmetric supercapacitors, *Appl. Surf. Sci.* 413 (2017) 351–359. <https://doi.org/10.1016/j.apsusc.2017.04.067>.
- [26] B. Cai, M. Zhao, Y. Ma, Z. Ye, J. Huang, Bio-inspired Formation of 3D Hierarchical CoFe₂O₄ Porous Microspheres for Magnetic Controlled Drug Release, *ACS Appl. Mater. Interfaces.* 7 (2015) 1327-1333. <https://doi.org/10.1021/am507689a>.
- [27] D. Mukherjee, T. Dhakal, M. H. Phan, H. Srikanth, P. Mukherjee, S. Witanachchi, Role of crystal orientation on the magnetic properties of CoFe₂O₄ thin films grown on Si (100) and Al₂O₃ (0001) substrates using pulsed laser deposition, *Physica. B. Condens. Matter.* 406 (2011) 2663-2668. <https://doi.org/10.1016/j.physb.2011.03.080>.
- [28] T. Dhakal, D. Mukherjee, R. Hyde, P. Mukherjee, M. H. Phan, H. Srikanth, S. Witanachchi, Magnetic anisotropy and field switching in cobalt ferrite thin films deposited by pulsed laser ablation, *J. Appl. Phys.* 107 (2010) 053914. <https://doi.org/10.1063/1.3327424>.
- [29] W. Huang, J. Zhu, H. Z. Zeng, X. H. Wei, Y. Zhang, Y. R. Li, Strain induced magnetic anisotropy in highly epitaxial CoFe₂O₄ thin films, *Appl. Phys. Lett.* 89 (2006) 262506. <https://doi.org/10.1063/1.2424444>.
- [30] J. de la Figuera, A. Quesada, L. Martín-García, M. Sanz, M. Oujia, M. Castillejo, A. Mascaraque, A. T. N'Diaye, M. Foerster, L. Aballe, J. F. Marco, Mössbauer and Magnetic Properties of Coherently Mixed Magnetite-Cobalt Ferrite Grown by Infrared Pulsed-Laser Deposition, *Croat. Chem. Acta* 88 (4) (2015) 453–460. <https://doi.org/10.5562/cca2752>.
- [31] M. Khodaei, S. A. S. Ebrahimi, Y. J. Park, J. M. Ok, J. S. Kim, J. Son, S. Baik, Strong in-plane magnetic anisotropy in (111)-oriented CoFe₂O₄ thin film, *J. Magn. Mater.* 340 (2013) 16–22. <https://doi.org/10.1016/j.jmmm.2013.03.019>.
- [32] J. G. Lee, K. P. Chae, J. C. Sur, Surface morphology and magnetic properties of CoFe₂O₄ thin films grown by a RF magnetron sputtering method, *J. Magn. Mater.* 267 (2003) 161–167. [https://doi.org/10.1016/S0304-8853\(03\)00348-2](https://doi.org/10.1016/S0304-8853(03)00348-2).
- [33] N. C. Pramanik, T. Fujii, M. Nakanishi, J. Takada, Development of Co_{1+x} Fe_{2-x}O₄ (x= 0-0.5) thin films on SiO₂ glass by the sol-gel method and the study of the effect of composition on their magnetic properties, *Mater. Lett.* 59 (2005) 88-93. <https://doi.org/10.1016/j.matlet.2004.09.023>.
- [34] H. M. Pahtan, S. S. Kale, C. D. Lokhande, S. H. Han, O. S. Joo, Preparation and characterization of amorphous manganese sulfide thin films by SILAR method, *Mater. Res. Bull.* 42 (2007) 1565-1569. <https://doi.org/10.1016/j.materresbull.2006.11.017>.

- [35] S. S. Bellad, C. H. Bhosale, Substrate temperature dependent properties of sprayed CoFe₂O₄ ferrite thin films, *Thin Solid Films* 322 (1998)93–97. [https://doi.org/10.1016/S0040-6090\(97\)00962-0](https://doi.org/10.1016/S0040-6090(97)00962-0).
- [36] M.A. Almessiere, A.V. Trukhanov, Y. Slimani, K.Y. You, S.V. Trukhanov, E.L. Trukhanova, F. Esa, A. Sadaqat, K. Chaudhary, M. Zdorovets, A. Baykal, Correlation between composition and electrodynamic properties in nanocomposites based on hard/soft ferrimagnetics with strong exchange coupling, *Nanomaterials-Basel* 9 (2019) 202. <https://doi.org/10.3390/nano9020202>.
- [37] M.V. Zdorovets, A.L. Kozlovskiy, Study of the effect of La³⁺ doping on the properties of ceramics based on BaTiO_x, *Vacuum* 168 (2019) 108838. <https://doi.org/10.1016/j.vacuum.2019.108838>.
- [38] T.I. Zubar, V.M. Fedosyuk, A.V. Trukhanov, N.N. Kovaleva, K.A. Astapovich, D.A. Vinnik, E.L. Trukhanova, A.L. Kozlovskiy, M.V. Zdorovets, A.A. Solobai, D.I. Tishkevich, S.V. Trukhanov, Control of growth mechanism of electrodeposited nanocrystalline NiFe films, *J. Electrochem. Soc.* 166 (2019) D173-D180. <https://doi.org/10.1149/2.1001904jes>.
- [39] T. Zubar, A.V. Trukhanov, D. Vinnik, K. Astapovich, D.I. Tishkevich, E. Kaniukov, A. Kozlovskiy, M. Zdorovets, S.V. Trukhanov, The Features of the growth processes and magnetic domain structure of NiFe nano-objects, *J. Phys. Chem. C* 123 (2019) 26957-26964. <https://doi.org/10.1021/acs.jpcc.9b06997>.
- [40] A. Hannachi, S. Hammami, N. Raouafi, H. Maghraoui-Meherzi, Preparation of manganese sulfide (MnS) thin films by chemical bath deposition: Application of the experimental design methodology, *J. Alloys Compd.* 663 (2016) 507-515. <https://doi.org/10.1016/j.jallcom.2015.11.058>.
- [41] R. S. Mane, C. D. Lokhande, Chemical deposition method for metal chalcogenide thin films, *Mater. Chem. Phys.* 65 (2000) 1-31. [https://doi.org/10.1016/S0254-0584\(00\)00217-0](https://doi.org/10.1016/S0254-0584(00)00217-0).
- [42] X. Qu, Statistical properties of Rechtschaffner designs, *J. Stat. Plan. Inference.* 137 (2007) 2156 – 2164. <https://doi.org/10.1016/j.jspi.2006.06.042>.
- [43] Mathieu, D., Luu, R. P. T., 1980. Software NEMROD, Université d'Aix-Marseille III, France.
- [44] N. Hosni, N. Bouaniza, W. Selmi, K. Assili, H. Maghraoui-Meherzi, Synthesis and physico-chemical investigations of AgSbS₂ thin films using Doehlert design and under DFT framework, *J. Alloys Compd.* 778 (2018) 913-923. <https://doi.org/10.1016/j.jallcom.2018.11.072>.
- [45] P. D. Haaland, *Experimental Design in Biotechnology*, Marcel Dekker, New York, 1989.
- [46] A. Kesraoui Abdessalem, N. Oturan, N. Bellakhal, M. Dachraoui, M. A. Oturan, Experimental design methodology applied to electro-Fenton treatment for degradation of herbicide chlortoluron, *Appl. Catal. B Environ.* 78 (2008) 334-341. <https://doi.org/10.1016/j.apcatb.2007.09.032>.
- [47] N. Hosni, K. Zehani, R. Pires Brazuna, J. Moscovici, L. Bessais, H. Maghraoui-Meherzi, Synthesis of (2D) MNPs nanosheets of nickel ferrite using a low-cost co-precipitation process. *Mater. Sci. Eng., B.* 232 (2018) 48-54. <https://doi.org/10.1016/j.mseb.2018.10.012>.
- [48] S.V. Trukhanov, L.S. Lobanovski, M.V. Bushinsky, V.V. Fedotova, I.O. Troyanchuk, A.V. Trukhanov, V.A. Ryzhov, H. Szymczak, R. Szymczak, M. Baran, Study of A-site ordered PrBaMn₂O₆-δ

manganite properties depending on the treatment conditions, *J. Phys.: Condens. Matter* 17 (2005) 6495-6506. <https://doi.org/10.1088/0953-8984/17/41/019>.

[49] M.V. Zdorovets, A. Arbutov, A.L. Kozlovskiy, Synthesis of LiBaZrOx ceramics with a core-shell structure, *Ceram. Int.* 46 (2020) 6217-6221. <https://doi.org/10.1016/j.ceramint.2019.11.090>.

[50] S.V. Trukhanov, Peculiarities of the magnetic state in the system $\text{La}_{0.70}\text{Sr}_{0.30}\text{MnO}_3$ - γ ($0 \leq \gamma \leq 0.25$), *JETP* 100 (2005) 95-105. <https://doi.org/10.1134/1.1866202>.

[51] M.V. Zdorovets, A.L. Kozlovskiy, Study of the stability of the structural properties of CeO₂ microparticles to helium irradiation, *Surf. Coat. Techn.* 383 (2020) 125286. <https://doi.org/10.1016/j.surfcoat.2019.125286>.

[52] S.V. Trukhanov, I.O. Troyanchuk, A.V. Trukhanov, I.M. Fita, A.N. Vasil'ev, A. Maignan, H. Szymczak, Magnetic properties of $\text{La}_{0.70}\text{Sr}_{0.30}\text{MnO}_{2.85}$ anion-deficient manganite under hydrostatic pressure, *JETP Lett.* 83 (2006) 33-36. <https://doi.org/10.1134/S0021364006010085>.

[53] A. Kozlovskiy, I. Kenzhina, M. Zdorovets, Synthesis, phase composition and magnetic properties of double perovskites of $\text{A}(\text{FeM})\text{O}_{4-x}$ type ($\text{A}=\text{Ce}$; $\text{M}=\text{Ti}$), *Ceram. Int.* 45 (2019) 8669-8676. <https://doi.org/10.1016/j.ceramint.2019.01.187>.

[54] J. Zhang, F. Liu, J. P. Cheng, X. B. Zhang, Binary Nickel-cobalt Oxides Electrode Materials for High-performance Supercapacitors: Influence of its Composition and Porous Nature, *ACS Appl. Mater. Interfaces.* 7 (2015) 17630-17640. <https://doi.org/10.1021/acsami.5b04463>.

[55] F. Rigato, J. Geshev, V. Skumryev, J. Fontcuberta, The magnetization of epitaxial nanometric CoFe_2O_4 (001) layers, *J. Appl. Phys.* 106 (2009) 113924. <https://doi.org/10.1063/1.3267873>.

[56] C. Jin, H. Liu, P. Li, D. F. Kuang, H. L. Bai, Anomalous magnetic properties of the epitaxial CoFe_2O_4 films prepared by reactive cosputtering, *J. Appl. Phys.* 110 (2011) 013917. <https://doi.org/10.1063/1.3608041>.

[57] S. Matzen, J.-B. Moussy, R. Mattana, F. Petroff, C. Gatel, B. Warot-Fonrose, J. C. Cezar, A. Barbier, M.-A. Arrio, P.H. Sainctavit, Restoration of bulk magnetic properties by strain engineering in epitaxial CoFe_2O_4 (001) ultrathin films, *Appl. Phys. Lett.* 99 (2011) 052514. <https://doi.org/10.1063/1.3622307>.

[58] H. Yanagihara, K. Uwabo, M. Minagawa, E. Kita, N. Hirota, Perpendicular magnetic anisotropy in CoFe_2O_4 (001) films epitaxially grown on MgO (001), *J. Appl. Phys.* 109 (2011) 07C122. <https://doi.org/10.1063/1.3566079>.

[59] M. Ning, J. Li, C.K. Ong, S.J. Wang, High perpendicular coercive field of (100)-oriented CoFe_2O_4 thin films on Si (100) with MgO buffer layer, *J. Appl. Phys.* 103 (2008) 013911. <https://doi.org/10.1063/1.2828040>.

Highlights

- 3D-CoFe₂O₄ nanoflowers thin films was successfully synthesized by low-cost chemical bath deposition (CBD) process
- Rechtschaffner design has been applied to investigate the influence of the principal experimental parameters on saturation magnetization.
- Doehlert matrix has been used to predict the optimal condition of the saturation magnetization.
- The obtained 3D-CoFe₂O₄ nanoflowers thin film could be useful for supercapacitor application.

Journal Pre-proof